

A Study of Dispersed Phenomena on Rushton and Rushton V-CUT

Varit Kunopagarnwong¹, Wisarut Manasthammakul², Thongchai Rohitatisa Srinophakun^{1,*}

¹ Department of Chemical Engineering, Faculty of Engineering, Kasetsart University, Bangkok, 10900, Thailand.

² Center of Excellence for Petroleum, Petrochemicals and Advanced Materials, Pathumwan, Bangkok 10330, Thailand

*Corresponding author's email: fengtc [AT] hotmail.com

ABSTRACT— *The flow behavior of liquid-solid particles in mixing tanks using a modified Rushton impeller, called a Rushton V-cut impeller, was studied. Both the Rushton and Rushton V-cut impellers were compared at a 300 rpm stirring speed and a 10 % wt solid concentration. Hydrodynamic behaviors, such as solid volume fraction, velocity, pressure, and shear stress, in both the Rushton and Rushton V-cut impellers were investigated. Computational fluid dynamics (CFD) software able to understanding of hydrodynamics of stirring liquids which contain solid particles. CFD programme was to predict the mixing flow of the highly viscous system. Therefore, the present work was carried out using CFD software with the Eulerian-Eulerian approach with a turbulent k-ε model. The simulation of mixing tanks was consisted of moving and stationary zones by using moving references frame method or MFR. The results were observed that Rushton V-cut can dramatically reduce pressure up to 20% and the shear stress up to 64.38% while keeping the liquid-solid mixing at a considerable degree. Therefore, this design can reduce the power consumption.*

Keywords— Computational fluid dynamics (CFD), Rushton impeller, and Flow behavior

1. INTRODUCTION

In industrial process engineering, i.e. pharmaceuticals and cosmetics (Blais and Bertrand, 2017), mixing is a unit operation whereby a heterogeneous physical system is manipulated to make it more homogeneous. Typical examples of mixing processes in the industry include concrete mixing, where sand, small stones or gravel, and water are mixed to a homogeneous self-hardening mass, and used in the construction industry. The other classical mixing process is mulling foundry molding sand, where sand, clay, fine coal dust and water are mixed. Mixing tanks are required to fulfill several needs, including miscible liquid blending, suspending solid particles in a liquid phase, and the dispersion of gas or immiscible liquids in a liquid phase. They are also used in many multi-phase systems such as in catalytic reactions, leaching, and polymerization. These processes are costly and time-consuming, therefore computational fluid dynamics (CFD) is a powerful technique for analysis and design.

Commercial CFD software can aid in the understanding of the hydrodynamic behavior of stirring liquids which contain solid particles, such as in drug coating [1], or gas-solid flow, such as in fluid catalytic cracking (FCC) and combustion processes [2, 3, 4]. This software can also predict the mixing flow of highly viscous systems, such as fermentation processes [5]. The Eulerian model approach for multiphase flow, or the two-fluid model, is normally used for predicting the dynamic behavior of the fluid-particle system [6]. The turbulence model, with the $k-\epsilon$ model, is one of the most common for simulating flow characteristics and mixing properties for turbulent flow conditions [7, 8]. Impeller type is significant to mixing behavior because the right flow pattern is critical to achieving the desired result. The blades or impellers are an important factor to design for solid-liquid mixing [9, 10]. The force is required to induce a moving blade and then through solid particles mixed with liquid. Moreover, the design of the impeller also affects the mixing characteristics of the stirring tank. For example, a coaxial mixer consists of an outer anchor and an inner Rushton turbine. It is suitable for high viscosity or pseudo-plastic mixing, and its large double-blade impeller can achieve a better micromixing performance [11]. Many studies have used CFD to predict the behavior of liquid-solid systems. Several studies have been published investigating the hydrodynamics of mixing flow inside stirring tanks using a Rushton impeller [12, 13]. Most of these reports focused on commercial four and six blades Rushton impellers, while very little

has been reported on Rushton blades with V-cuts. The major objective of this work is to use simulations to calculate the effect of stirring liquids containing solid particles, with a Rushton impeller or a Rushton V-cut impeller.

2. MATERIALS AND METHODS

Calculations were carried out using the ANSYS FLUENT 12.1 software on the WATA cluster (The high-performance computer system at the faculty of engineering at Kasetsart University: IBM xSeries and Blade series HS-22, CPU Intel Quad-Core Xeon E5540, 2.53 GHz, RAM 8 GB).

2.1 Simulated mixing tank geometry

This work considers the pattern of fluid flow in a 3D oval or elliptical bottom cylinder tank as shown in Figure 1. The flow of the solid-liquid mixture is calculated and analyzed during the simulation. The geometry of the riser section used in the present simulation is shown in Figure 2. The simulated mixing tank is 24 cm high and 24 cm in diameter, with four baffles and two different types of impellers (Rushton and Rushton V-cut). The 3D geometry of the mixing tank with meshing is generated by a general meshing technique. The overview of the grid system, and the configuration of the mixing tank, used in this work is shown in Figure 3. This method provides a better resolution of the velocity field near the wall.

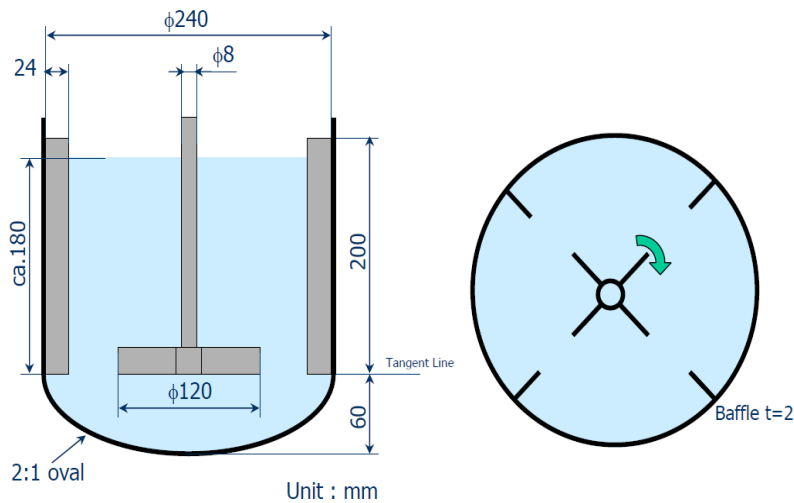


Figure 1: Geometry of the reactor simulated in this work

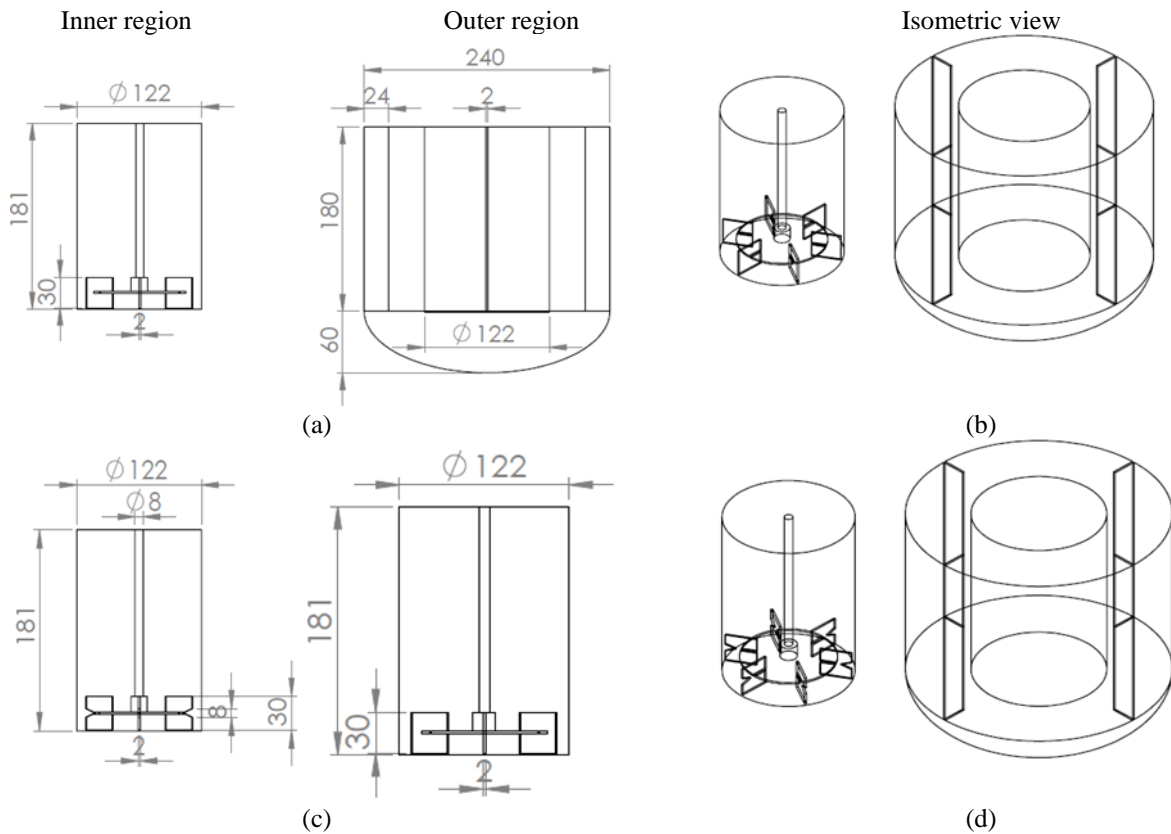


Figure 2: Geometry of (a) and (b) Rushton design, (c) and (d) Rushton V-cut blade design

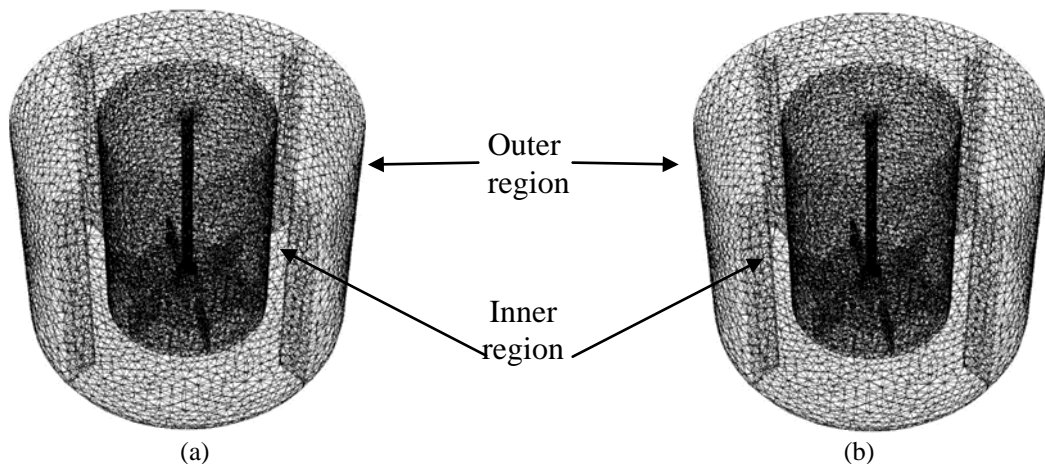


Figure 3: Schematic drawing of 3D mixing tank with triangular elements used in the geometry meshing: (a) Rushton and (b) Rushton V-cut

There are two parts of the geometry, the inner region and the outer region. The inner region is a cylindrical shape that contains the blade inside. In the simulation, this part is rotated, affecting the outer region. The outer region is the tank that contains the inner region. The advantage of splitting the mixing tank into two designated regions is that it becomes easy to select the boundaries in the meshing method. This meshing method is used moving references frame or MRF [14].

2.2 Modeling the solid-liquid in the mixing tank

The mathematical model used by the simulation is based on a liquid-solid multiphase flow model. The homogeneous model in Eulerian–Eulerian multiphase flow, as applied to the two-phase liquid-solid flow, is used in this work. This means that the laws of conservation of mass and momentum are satisfied by each phase individually [15]. Standard

equations for single-phase flow (mass and momentum conservation equations) were used in the simulation. Considering the magnitude of the pressure drop across the grid, compressible fluid equations are necessary. Under usual operating conditions, the flow is found to be turbulent due to the Reynold number equals to 2.03×10^4 . In addition, solid-liquid mixing is most focused on agitation speed required to suspend the particles in the turbulent regime [16]. Turbulent stresses are modeled using the $k - \varepsilon$ model. The dependent variables are solved for each phase separately.

The Eulerian multiphase model allows for the modeling of multiple separate, yet interacting, phases. The phases can be liquid, gas, or solid, in nearly any combination. A Eulerian treatment is used for each phase, which is in contrast to the Eulerian-Lagrangian treatment that is used for the discrete phase model. With the Eulerian multiphase model, the number of secondary phases is limited only by memory requirements and convergence behavior. Any number of secondary phases can be modeled, provided that sufficient memory is available. For complex multiphase flows, however, the solution is limited by convergence behavior. The Eulerian multiphase model does not distinguish between fluid-fluid and fluid-solid (granular) multiphase flows. A granular flow is simply one that involves at least one phase that has been designated as a granular phase.

2.3 Volume fraction equation

The description of multiphase flow as interpenetrating continua incorporates the concept of phasic volume fractions, denoted here by α_q . Volume fractions represent the space occupied by each phase, and the laws of conservation of mass and momentum are satisfied by each phase individually. The derivation of the conservation equations can be done by ensemble averaging the local instantaneous balance for each of the phases. In the simulation, a solid value in volume fraction is shown, so it must find a relation between the mass of solid and solid volume fraction.

The volume of phase q , V_q , is defined by:

$$V_q = \int_V \alpha_q dV \quad (1)$$

where:

$$\sum_{q=1}^n \alpha_q = 1 \quad (2)$$

The effective density of phase q is:

$$\hat{\rho}_q = \alpha_q \rho_q \quad (3)$$

2.4 Conservation Equation

The general conservation equations from which the equations solved by ANSYS FLUENT are derived and presented in this section, followed by the solved equations.

The continuity of mass for phase q is:

$$\frac{\partial}{\partial t} (\alpha_q \rho_q) + \nabla \cdot (\alpha_q \rho_q \vec{v}_q) = \sum_{p=1}^n (\dot{m}_{pq} - \dot{m}_{qp}) + S_q \quad (4)$$

where \vec{v}_q is the velocity of phase q and \dot{m}_{pq} characterizes the mass transfer from the p^{th} to q^{th} phase, and \dot{m}_{qp} characterizes the mass transfer from phase q to phase p , and it is able to specify these mechanisms separately.

By default, the source term S_q on the right-hand side of Equation (4) is zero, but it can specify a constant or user-defined mass source for each phase.

The conservation of momentum for phase q yields:

$$\frac{\partial}{\partial t}(\alpha_q \rho_q \mathcal{V}_q) + \nabla \cdot (\alpha_q \rho_q \mathcal{V}_q) = -\alpha_q \nabla p + \nabla \cdot \bar{\bar{\tau}}_q + \alpha_q \rho_q \mathcal{G} + \sum_{p=1}^n (K_{pq}^p + m_{pq}^p \mathcal{V}_{pq} - m_{qp}^p \mathcal{V}_{qp}) + (F_q^p + F_{lift,q}^p + F_{vm,q}^p) \quad (5)$$

where $\bar{\bar{\tau}}_q$ is the q^{th} phase stress-strain tensor:

$$\bar{\bar{\tau}}_q = \alpha_q \mu_q (\nabla \mathcal{V}_q + \nabla \mathcal{V}_q^T) + \alpha_q (\lambda_q - \frac{2}{3} \mu_q) \nabla \cdot \mathcal{V}_q \mathbf{I} \quad (6)$$

Here μ_q and λ_q are the shear and bulk viscosity of phase q , F_q^p is an external body force, $F_{lift,q}^p$ is a lift force, $F_{vm,q}^p$ is a virtual mass force, K_{pq}^p is an interaction force between phases, and p is the pressure shared by all phases.

\mathcal{V}_{pq} is the interphase velocity, defined as following. If $m_{pq}^p > 0$ (i.e., phase p mass is being transferred to phase q), $\mathcal{V}_{pq} = \mathcal{V}_q$; if $m_{pq}^p < 0$ (i.e., phase q mass is being transferred to phase p), $\mathcal{V}_{pq} = \mathcal{V}_p$. Likewise, if $m_{qp}^p > 0$ then $\mathcal{V}_{qp} = \mathcal{V}_q$, if $m_{qp}^p < 0$ then $\mathcal{V}_{qp} = \mathcal{V}_p$. Equation 5 must be closed with appropriate expressions for the interphase force K_{pq}^p . This force depends on the friction, pressure, cohesion, and other effects, and is subject to the conditions that $K_{pq}^p = -K_{qp}^p$ and $-K_{qq}^p = 0$.

ANSYS FLUENT uses a simple interaction term of the following form:

$$\sum_{p=1}^n K_{pq}^p = \sum_{p=1}^n K_{pq} (\mathcal{V}_p - \mathcal{V}_q) \quad (7)$$

where K_{pq} ($= K_{qp}$) is the interphase momentum exchange coefficient

The continuity equation is considered in the conservation of mass. The volume fraction of each phase is calculated from a continuity equation:

$$\frac{1}{\rho_{rq}} \left(\frac{\partial}{\partial t} (\alpha_q \rho_q) + \nabla \cdot (\alpha_q \rho_q \mathcal{V}_q) \right) = \sum_{p=1}^n (m_{pq}^p - m_{qp}^p) \quad (8)$$

where ρ_{rq} is the phase reference density, or the volume averaged density of the q^{th} phase in the solution domain.

2.5 Fluid-Solid Momentum Equations

The system uses a multi-fluid granular model to describe the flow behavior of a fluid-solid mixture. The solid-phase stresses are derived by making an analogy between the random particle motion arising from particle-particle collisions and the thermal motion of molecules in a gas, taking into account the inelasticity of the granular phase. As is the case for a gas, the intensity of the particle velocity fluctuation determines the stresses, viscosity, and pressure of the solid phase. The kinetic energy associated with the particle velocity fluctuations is represented by a “pseudo-thermal” or granular temperature which is proportional to the mean square of the random motion of particles.

The conservation of momentum:

$$\frac{\partial}{\partial t}(\alpha_s \rho_s \bar{v}_s) + \nabla \cdot (\alpha_s \rho_s \bar{v}_s \bar{v}_s) = -\alpha_s \nabla p + \nabla \cdot \bar{\tau}_s + \alpha_s \rho_s \bar{g} + \sum_{p=1}^n (K_{ls} (\bar{v}_l - \bar{v}_s) + m_{ls} \bar{v}_l - m_{sl} \bar{v}_s) + (F_s + F_{lift,s} + F_{vm,s}) \quad (9)$$

where ρ_s is the s^{th} solids pressure, $K_{ls} = K_{sl}$ is the momentum exchange coefficient between fluid or solid phase l and solid phase s , N is the total number of phases.

2.5.1 Fluid-Solid Exchange Coefficient

The fluid-solid exchange coefficient K_{sl} is the value to show interphase relation between fluid and solid in a system, it can be written in the following general form:

$$K_{sl} = \frac{\alpha_s \rho_s f}{\tau_s} \quad (10)$$

where f is defined differently for the different exchange-coefficient models (as described below), and τ_s , the “particulate relaxation time”, is defined as

$$\tau_s = \frac{\rho_s d_s^2}{18\mu_l} \quad (11)$$

where d_s is the diameter of particles of phase s .

All definitions of f include a drag function (C_D) that is based on the relative Reynolds number (Re_s). It is this drag function that differs among the exchange-coefficient models.

2.5.2 Gidaspow Drag Model

For very dense gas-solid or liquid-solid flows, the Gidaspow correlation is recommended as following:

$$K_{sl} = \frac{3}{4} C_D \frac{\alpha_s \alpha_l \rho_l |\bar{v}_s - \bar{v}_l|}{d_s} \alpha_l^{-2.65} \quad \alpha_l > 0.8 \quad (12a)$$

where $C_D = \frac{24}{\alpha_l Re_s} [1 + 0.15(\alpha_l Re_s)^{0.687}]$

$$K_{sl} = 150 \frac{\alpha_s (1 - \alpha_l) \mu_l}{\alpha_l d_s^2} + 1.75 \frac{\rho_l \alpha_s |\bar{v}_s - \bar{v}_l|}{d_s} \quad r_c < 0.8 \quad (12b)$$

2.5.3 Solid Pressure Forces

Additional solids pressure and solids stress terms are introduced into the solid phase momentum equations to account for forces due to solid collisions:

$$\frac{\partial}{\partial t}(\alpha_s P_s U_s) + \nabla \cdot (\alpha_s (P_s U_s \otimes U_s)) = -\alpha_s \nabla P_f - \nabla P_s + \nabla \cdot (\alpha_s \tau_s) + S_M + M_S \quad (13)$$

where P_f is the fluid phase pressure.

P_s is the solids pressure due to inter-particle collisions.

τ_s is stress tensor due to inter-particle collisions.

S_M describes momentum sources due to external body forces and user defined momentum sources acting on the solid phase.

M_s describes interfacial forces acting on the solid phase due to interactions with other phases (e.g. drag).

2.5.4 The $k - \varepsilon$ model

The present work $k - \varepsilon$ model is employed to carried out in the turbulent flow into CFD model for solid-liquid phases [17] because the fluid, water, is less viscosity leading to the behavior of fluid as stratified flow. Thus $k - \varepsilon$ model is appropriated in this study. k is the turbulence kinetic energy and defined as the variance of the fluctuations in velocity. ε is the turbulence eddy dissipation; the rate at which the velocity fluctuations dissipate.

The $k - \varepsilon$ model introduces two new variables into the system of equations. The continuity equation is then:

$$\frac{\partial \rho}{\partial t} + \nabla \cdot (\rho U) = 0 \quad (14)$$

and the momentum equation becomes:

$$\frac{\partial \rho U}{\partial t} + \nabla \cdot (\rho U \otimes U) - \nabla \cdot (\mu_{eff} \nabla U) = \nabla p' + \nabla \cdot (\mu_{eff} \nabla U)^T + B \quad (15)$$

where B is the sum of body forces, μ_{eff} is the effective viscosity accounting for turbulence, and p' is the modified pressure given by

$$p' = p + \frac{2}{3} \rho k \quad (16)$$

The $k - \varepsilon$ model, like the zero equation model, is based on the eddy viscosity concept, so that

$$\mu_{eff} = \mu + \mu_t \quad (17)$$

where μ_t is the turbulence viscosity.

The $k - \varepsilon$ model assumes that the turbulence viscosity is linked to the turbulence kinetic energy and dissipation via the relation

$$\mu_t = C_\mu \rho \frac{k^2}{\varepsilon} \quad (18)$$

where C_μ is constant.

The values of k and ε come directly from the differential transport equations for the turbulence kinetic energy and turbulence dissipation rate:

$$\frac{\partial(\rho k)}{\partial t} + \nabla \cdot (\rho U k) = \nabla \cdot \left[\left(\mu + \frac{\mu_t}{\sigma_k} \right) \nabla k \right] + P_k - \rho \varepsilon \quad (19)$$

$$\frac{\partial(\rho\varepsilon)}{\partial t} + \nabla \bullet (\rho U \varepsilon) = \nabla \bullet \left[\left(\mu + \frac{\mu_t}{\sigma_\varepsilon} \right) \nabla \varepsilon \right] + \frac{\varepsilon}{k} (C_{\varepsilon 1} P_k - C_{\varepsilon 2} \rho \varepsilon) \quad (20)$$

where $C_{\varepsilon 1}$, $C_{\varepsilon 2}$, σ_k and σ_ε are constants. P_k is the turbulence production due to viscous and buoyancy forces, which is modeled using:

$$P_k = \mu_t \nabla U \bullet (\nabla U + \nabla U^T) - \frac{2}{3} \nabla \bullet U (3\mu_t \nabla \bullet U + \rho k) + P_{kb} \quad (21)$$

For incompressible flow, $\nabla \bullet U$ is small and the second term on the right side of Equation (22) does not contribute significantly to the production. For compressible flow, $\nabla \bullet U$ is only large in regions with high velocity divergence, such as at shocks.

The term $3\mu_t$ in Equation (22) is based on the “frozen stress” assumption. This prevents the values of k and ε becoming too large through shocks, a situation that becomes progressively worse as the mesh is refined at shocks. The expert parameter compressible turbulence production factor can be used to set the value of the factor in front of μ_t , the default value is 3, as shown.

If the full buoyancy model is being used, the buoyancy production term P_{kb} is modeled as:

$$P_{kb} = \frac{\mu_t}{Pr_t} g \bullet \nabla \rho \quad (22)$$

If the Boussinesq buoyancy model is being used, it is:

$$P_{kb} = \frac{\mu_t}{Pr_t} \rho \beta g \bullet \nabla T \quad (23)$$

2.5.5 Meshing and simulation for solid-liquid in mixing tank

The problem is divided into many grids and the calculation of fluid phenomena is carried out in each grid. This process is referred to as “meshing”. The Tri-angular element is selected for the geometry meshing. Meshing is an important step for selecting boundary conditions. The meshing is adjusted to provide a high resolution and generated using an infrastructure grid, as shown in Figure 3. Over 250,000 elements were used in each mixing tank to calculate the fluid phenomena. The grids are refined only near the impeller because this work is considered especially for hydrodynamics near the Rushton. Therefore the refine meshing are the wall is not necessary [18].

The differential equations in the mathematical model have solved on a unit volume basis. Thus, the conservations need to yield overall possible finite volumes covering the whole problem spaces. This method called finite volume technique. The differential equation expresses the conservation over infinitesimal control volumes.

The mixing tank is assumed to be symmetric, thus only one-quarter of the reactor is simulated. Calculations using both constant a solid volume fraction and varying the solid load have been performed. All the models use the following assumptions: the mixing tank is symmetric and the liquid-solid mixing is the same in every quarter, there are no reactions occurring in the mixing tank, the mixing tank walls are adiabatic, there is a non-slip condition for all rigid walls, the temperature in the tank is constant, and the mass is constant both before and after the mixing.

3. RESULTS AND DISCUSSION

Wisarat (2011) was carried out the solid-liquid mixture experiment in mixing vessel 10 L with blade Rushton at a solid concentration of 1%wt. The liquid and solid phases are water and aluminum oxide (Al_2O_3), respectively. Stirring speed is 300 rpm and mixed it until the mixture is well-mixed. The sampling 10 mL of a mixture will take out at 11 points as following Figure. 4. Comparing the results of solid concentration between experiment and simulation were obtained that the solid concentration of simulation result was almost the same to experimental data as shown in Figure 5.

Moreover, Figure. 6 showing the contour mixing between experiment and simulation at time 0 to 8 s with the same condition. The mixing of both methods is closed results. Therefore, the blade Rushton can be selected for as a case study with blade Rushton V-cut.

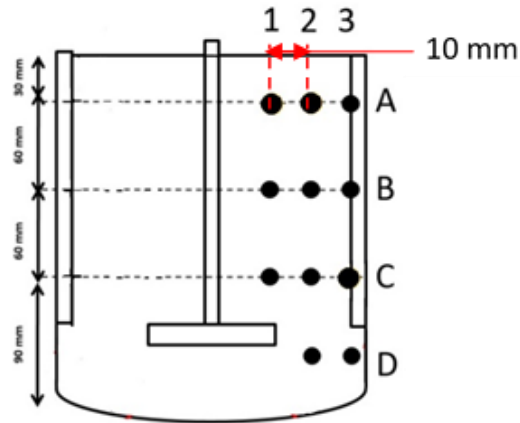


Figure 4: Collecting the position of the sampling

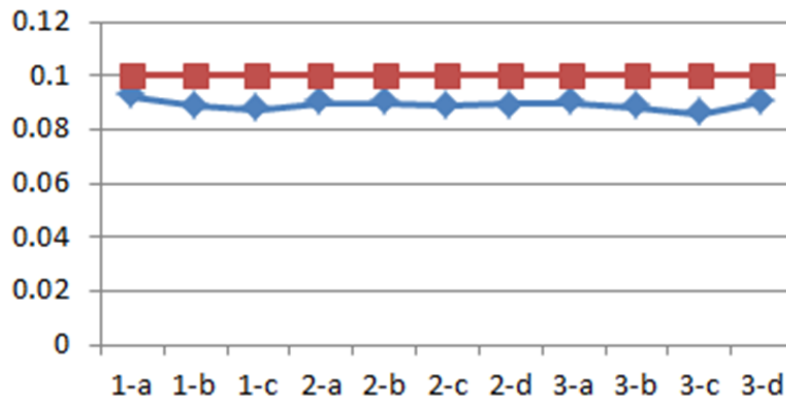


Figure 5: Simulation versus experimental data at 1%wt solid concentration and 300 rpm of stirring speed in Rushton blade

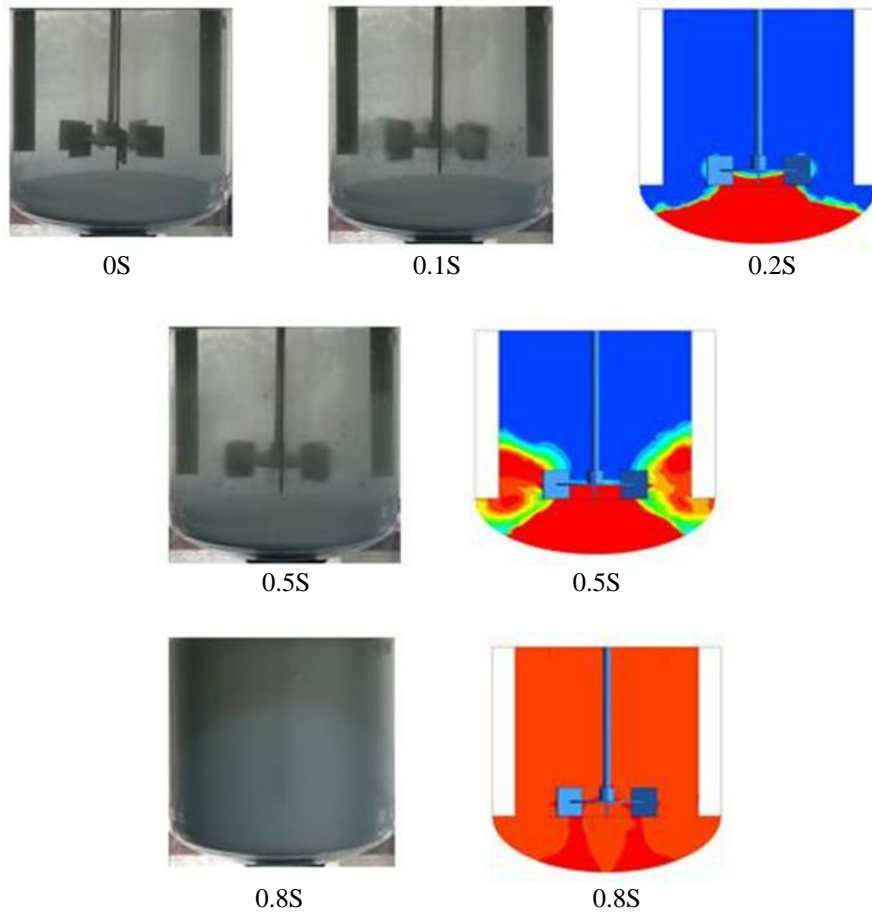


Figure 6: Comparing between experiment and simulation of mixing phenomena of water and Aluminum phases at time 0 to 8 s

The calculation results for the solid volume fraction, solid velocity profile, pressure profile and shear stress profile are shown in Figures. 7, 8, 9 and 10, respectively. A comparison of the solid volume fraction distribution of the Rushton and Rushton V-cut geometries at 300 rpm are shown in Figure 7. These results show that the distribution of the solid volume fraction was almost the same using both the Rushton and Rushton V-cut geometries. For both geometries, a high solid volume fraction was observed at the bottom of the tank and the distribution of solid volume fractions decreased slightly nearer to the container wall. These results show that the solid particles were mixed well and are close to experimental solid fraction results.

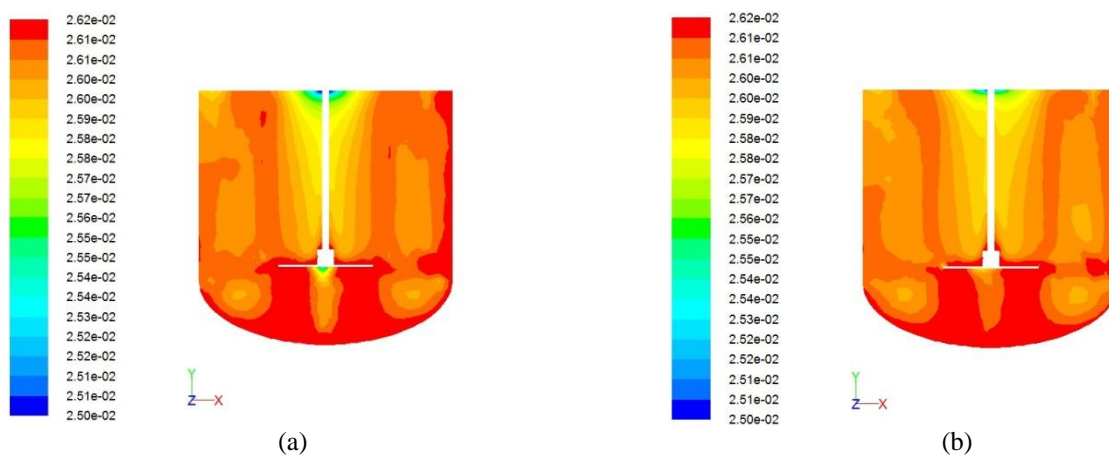


Figure 4: Simulated solid volume fraction: Rushton versus Rushton V-cut

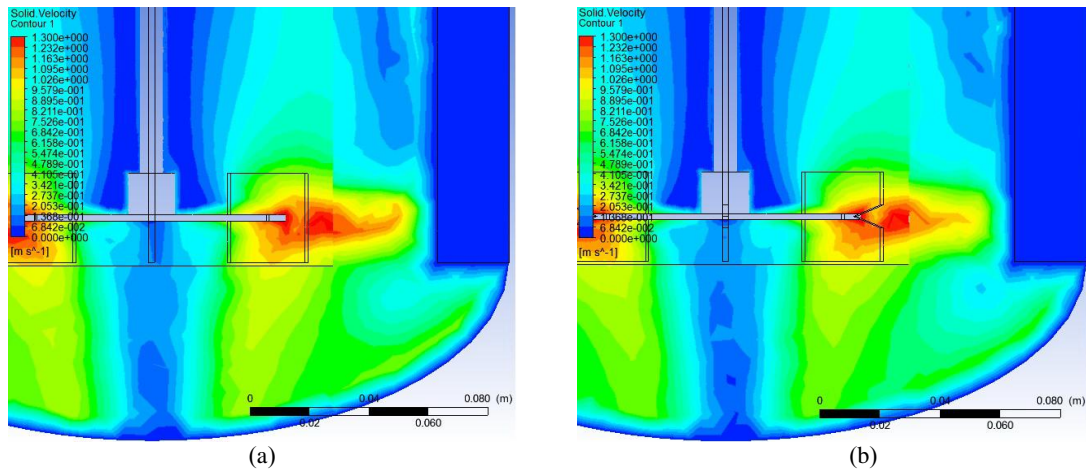


Figure 8: Simulated solid velocity profile (m/s): (a) Rushton, (b) Rushton V-cut

Figure 8 shows the results of the calculated solid velocity contours for the Rushton and Rushton V-cut geometries at 300 rpm. These results show that in both geometries, the velocity contours were almost the same. Low and high velocities were observed near the wall and blade regions, respectively.

The comparison of pressure contours in a mixing tank for the Rushton and Rushton V-cut geometries at 300 rpm are shown in Figure 9. High pressure was observed at the blades and baffles for both geometries. However, the pressure of 378.9 Pa at the Rushton V-cut blade was less than that for the Rushton blade of 473.7 Pa due to the cut in the blade at the high-pressure region. This has the effect of reducing the pressure in the tank. The benefit of pressure decreasing can be reduced the power consumption. The blades are cut in the region in which high pressure and high shear stress occur. Figure 10 shows that shear stress at blades is reduced from 0.235 Pa to 0.03789 Pa when the shape is changed from the Rushton to the Rushton V-cut blade.

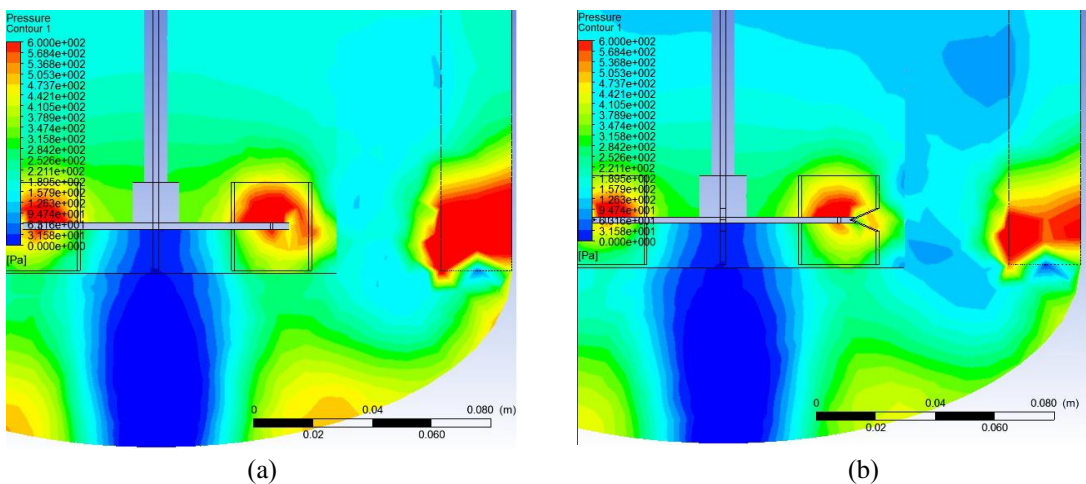


Figure 9: Pressure profile (Pascal) in simulation: (a) Rushton, (b) Rushton V-cut

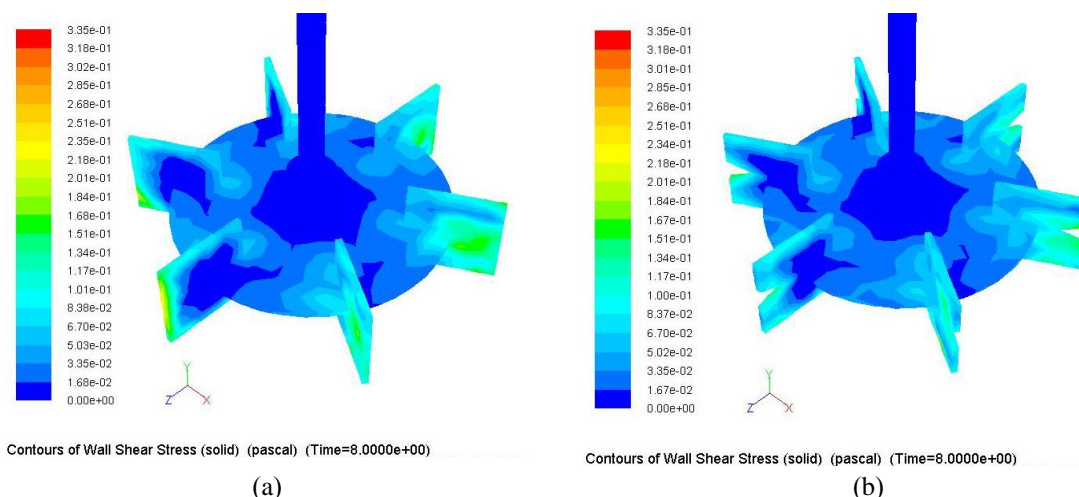


Figure 10: Shear stress (Pascal) in simulation: (a) Rushton, (b) Rushton V-cut

4. CONCLUSIONS

The blades designed for this system are a development on the Rushton blades. The Rushton V-cut blades are made by cutting a standard Rushton blade in the area that generates high pressure, or at the middle of the blades. This type of blade is called Rushton V-cut. Hydrodynamic simulations of solid dispersion were done in the mixing tank using ANSYS and the $k-\epsilon$ turbulent model. For both geometries, a low solid volume fraction was observed near the wall of the tank and a high solid volume fraction was observed near the bottom of the tank. These results show that the solid was mixed well, and are close to experimental results. The velocity contours of both geometries were almost the same. Low and high velocities were observed near the wall and blade regions, respectively. The simulated pressure profiles and shear stress profiles of the Rushton V-cut impeller were compared. The Rushton V-cut impeller can mix as well as the Rushton impeller. Moreover, at the Rushton V-cut blade, the pressure of 378.9 Pa was less than the Rushton blade of 473.7 Pa due to the cut in the blade at the high-pressure region with percent different of 20.01%. This has the effect of reducing the pressure in the tank. The blades are cut in the region in which high pressure and high shear stress occur. At blades, shear stress is reduced from 0.235 Pa to 378.9 Pa when the shape is changed from the Rushton to the Rushton V-cut blade. The percent difference is 64.38%. The benefit of pressure and shear stress decreasing can be reduced the power consumption.

5. ACKNOWLEDGEMENT

This research was supported by the Center of Excellence for Petroleum, Petrochemicals and Advanced Materials, Center for Advanced Studies in Industrial Technology, Department of Chemical Engineering, Faculty of Engineering, Kasetsart University.

6. REFERENCES

- [1] Fradette, L., P.A. Tanguy, F. Bertrand, F. Thibault, J.B. Ritz, E. Giraud, "CFD phenomenological model of solid-liquid mixing in stirred vessels", *Comput. and Chem. Eng.*, vol. 31, no. 4, pp. 334-345, 2007.
- [2] Zheng, Y., X. Wan, Z. Qian, F. Wei, Y. Jin, "Numerical simulation of the gas-particle turbulent flow in riser reactor based on $k-\epsilon-k_p-\epsilon_p-\Theta$ two-fluid model", *Chem. Eng. Sci.*, vol. 56 no. 24, pp. 6813-6822, 2001.
- [3] Zhou, L.X., L. Li, R.X. Li, and J. Zhang: "Simulation of 3-D gas-particle flows and coal combustion in a tangentially fired furnace using a two-fluid-trajectory model", *Powder Technol.*, vol. 125, pp. 226-233, 2012.
- [4] Das, A.K., J.D. Wilde, G.J. Heynderickx, G.B. Marin, J. Vierendeels, E. Dick, "CFD simulation of dilute phase gas-solid riser reactors: Part I – a new solution method and flow model validation", *Chem. Eng. Sci.*, vol. 59, no. 1, pp. 167-186, 2004.
- [5] Um, B.H., T.R. Hanley, "High-solid enzymatic hydrolysis and fermentation of solka floc into ethanol", *J. Microbiol. Biotechnol.*, vol. 18, no. 7, pp. 1257-1265, 2008.
- [6] Wadnerkar, D., M.O. Tade., V.K. Pareek, R.P. Utikar, "CFD simulation of solid-liquid stirred tanks for low dense solid loading systems", *Particuology.*, vol. 29, pp. 16-33, 2016.
- [7] Politano, M.S., P.M. Carrica, J. Converti, "A model for turbulent poly-disperse two-phase flow in vertical channels", *Int. J. Multiph. Flow*, vol. 29, no. 7, pp. 1153-1182, 2003.

- [8] Liu, B., H. Bolin, Z. Yanan, L. Jingliang, J. Zhijiang, “Numerical study on gas dispersion characteristics of a coaxial mixer with viscous fluids”, *J. Taiwan Inst. Chem. Eng.*, vol. 66, pp. 54-61, 2016.
- [9] Chandratilleke, G.R., A.B. Yu, J. Bridgwater, “A DEM study of mixing of particles induced by a flat blade”, *Chem. Eng. Sci.*, vol. 79, pp. 54-74, 2012.
- [10] Mousavi, S.M., P. Zamankhan, A. Jafari, “Computer simulations of sodium formate solution in a mixing tank”, *Commun. Nonlinear Sci. Numer. Simul.*, vol. 13, no. 2, pp. 380-399, 2008.
- [11] Liu, B., Y. Zhang, Y. Zheng, B. Huang, X. Chen, Z. Jin, “Micromixing simulation of novel large-double-blade impeller”, *J. Taiwan Inst. Chem. Eng.*, vol. 66, pp. 62-69, 2016.
- [12] Deglon, D.A., C.J. Meyer, “CFD modeling of stirred tanks: Numerical considerations”, *Miner Eng.*, vol. 19, no.10, pp. 1059-1068, 2006.
- [13] Kasat, G.R., A.R. Khopkar, V.V. Ranade, A.B. Pandit, “CFD simulation of liquid-phase mixing in solid-liquid stirred reactor”, *Chem. Eng. Sci.*, vol. 63, no. 15, pp. 3877-3885, 2008.
- [14] Ameer, H, “Mixing of complex fluids with flat and pitched bladed impeller: Effect of blade attack angle and shear thinning behavior”, *Food Bioprod. Process.*, vol. 99, pp. 71-77, 2016.
- [15] Gidaspow, D., R. Bezburaah, J. Ding, “Hydrodynamics of Circulating Fluidized Beds, Kinetic Theory Approach”, In *Fluidization VII, Proceedings of the 7th Engineering Foundation Conference on Fluidization*, 1992.
- [16] Lassaigne, M., B. Blais, L. Fradette, F. Bertrand, “Experimental investigation of the mixing of viscous liquids and non-dilute concentrations of particles in stirred tank”, *Chem. Eng. Res. Des.*, vol. 108, pp. 55-68, 2016.
- [17] Mishra, P., and F. Ein-Mozaffari, “Using computational fluid dynamics to analyze the performance of the maxbland impeller in solid-liquid mixing operations”, *Int. J. Multiphase Flow*, vol. 91, pp. 194-207, 2017.
- [18] Raj, R.T.K., A.D. Singh, S. Tare, S. Varma, S Varma, “Study of fluid Flow around Impeller Blades in Rushton turbine in a Baffled Vessel using Computational Fluid Dynamics”, *ARNP Journal of Engineering and Applied Sciences*, vol. 9, no. 5, pp. 659-666, 2014.